Mechanical and metallurgical properties of diffusion bonded AA2024 Al and AZ31B Mg

G. Mahendran[*1], V. Balasubramanian[2] and T. Senthilvelan[3]

[1]*IFET College of Engineering, Gangarampalayam, Villupuram Dt, Tamilnadu, India*
[2]*CEMAJOR, Annamalai University, Annamalai Nagar, Chidambaram, Tamilnadu, India*
[3]*Podicherry Engineering College, Puducherry, India*

Abstract. In the present study, diffusion bonding was carried out between AZ31B magnesium and AA2024 aluminium in the temperature range of $405^{\circ}C$ to $475^{\circ}C$ for 15 min to 85 min and 5 MPa to 20 MPa uniaxial loads was applied. Interface quality of the joints was assessed by microhardness and shear testing. Also, the bonding interfaces were analyzed by means of optical microscopy, scanning electron microscopy, energy dispersive spectrometer and XRD. The maximum bonding and shear strength was obtained at $440^{\circ}C$, 12 MPa and 70 min. The maximum hardness values were obtained from the area next to the interface in magnesium side of the joint. The hardness values were found to decrease with increasing distance from the interface in magnesium side while it remained constant in aluminium side. It was seen that the diffusion transition zone near the interface consists of various phases of $MgAl_2O_4$, Mg_2SiO_4 and Al_2SiO_5.

Keywords: diffusion bonding; bonding strength; shear strength; micro hardness; OM; SEM; XRD

1. Introduction

The light weight, high specific strength and recyclable characteristics of Mg alloys have recently attracted great attention in academic research and industry applications. There has been a growing interest in the diffusion bonding of magnesium and aluminium for aerospace and automotive applications (Li *et al.* 2007). This is a consequence not only of magnesium's relative density but also of its good damping characteristics, dimensional stability, machinability and low casting costs. Dissimilar welding of Mg and Al alloys would achieve weight reduction and high efficiency of production by a substitution of Mg alloy for Al alloy (Liu *et al.* 2006). However fusion welding of Mg and Al alloy always produces coarse grains and large brittle intermetallic compounds in the weld metal. Therefore, the welding of Mg/Al dissimilar materials by fusion welding is difficult (Juan *et al.* 2008). This hinders the development of the use of Mg and Al. However, the diffusion bonding of Mg/ Al dissimilar metals and the study of the phase constitution near the interface has not been reported. In this paper, the microstructure near the interface of diffusion bonded Mg/Al dissimilar materials were analysed using a scanning electron microscope (SEM). The phase constitution and lattice orientation relation in the Mg/Al diffusion zone were analysed by X-ray diffraction.

---

*Corresponding author, Ph.D., E-mail: mahe1967@yahoo.com

Table 1 Chemical composition of the base metal

Base metal	Si	Fe	Cu	Mn	Mg	Cr	Zn	Ti	Al	O	Pb	B	S
Aluminium (AA2024)	0.5	0.5	4.9	0.9	1.8	0.1	0.25	0.15	Bal	-	-	-	-
Magnesium (AZ31B)	-	-	-	0.2	Bal	-	1.0	-	3.0	-	-	-	-

Table 2 Mechanical properties of the base metal

Base material	Density (Kg/m³)	Ultimate tensile strength (MPa)	Elongation (%)	Shear strength (MPa)	Hardness (Hv) @ 50 g load
Aluminium (AA2024)	2.7×10^3	483	18	283	137
Magnesium (AZ31B)	1.77×10^3	255	21	145	75

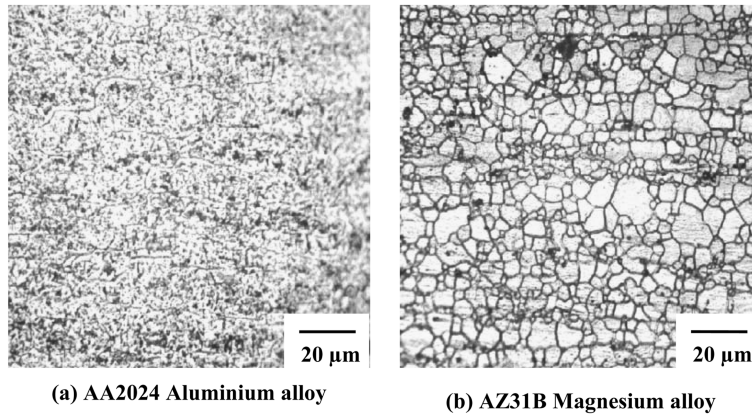(a) AA2024 Aluminium alloy (b) AZ31B Magnesium alloy

Fig. 1 Optical micrographs of the base materials

2. Experimental work

AZ31B Mg alloy and AA2024 Al alloy plates of 5 mm thickness were cut into the required dimensions (50×50 mm) by power hacksaw cutting and grinding. Chemical composition and mechanical properties of base materials are presented in Tables 1 and 2. Microstructure of the base materials are shown in Fig. 1. The polished and chemically treated specimens of a pair Mg/Al were stacked in a die made up of 316 L stainless steel and the entire diffusion bonding die setup, shown in Fig. 2 was inserted into a vacuum chamber. The heating chamber was fitted with super Kant Hal resistance heating wire band contains a water cooling coil to protect the O-rings and vacuum seals. The chamber is a PID (programmable interface device) controlled furnace with a maximum temperature of 1473 K at an accuracy of ±1 K. The temperature was measured using Platinum/ Platinum-Rhodium thermocouple and with a non-indicating safety controller.

The furnace is fitted with a removable bellows and a central shaft (Nimonic rod) that transmits the load to the specimens to be diffusion bonded. The central shaft has a groove along its length to suck
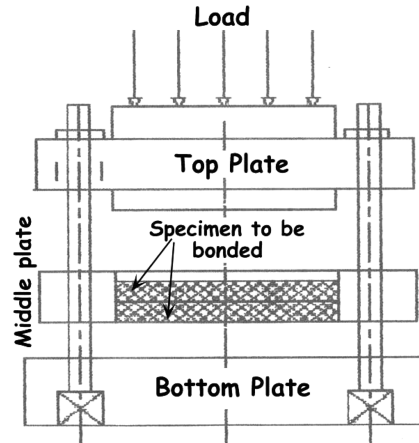
Fig. 2 Configuration of the diffusion bonding die setup

the air from the chamber. The bottom side is flat and can be fixed in the hydraulic press. The size of the inside chamber is 100 mm in die and 100 mm in height. The furnace is insulated with high quality; lightweight, ceramic fiber blankets to improve the efficiency of the system. The constant load or constant diffusion bonding pressure was applied using a servo-controlled hydraulic press. The maximum capacity of the press is 10 Ton. The pre determined pressure was applied using a pressure relief valve and the press was turned to auto mode after the load was reached. A pressure switch is actuated by turning the press to auto mode, which maintains the pressure level with an accuracy of $\pm100\,N$. A hydraulic ram transfers the load to the central shaft of the heating chamber and the specimens fixed in the dies. The load was measured using a load cell fixed in the hydraulic ram. Care was taken to fix the axis of the hydraulic ram and the central shaft of the heating chamber in linear axis. Water cooling is essential to maintain the temperature of the vacuum seals bellows at $473\,K$. The cooling system has two tanks connected to the heating chamber. The warm water (at $325\,K$) coming out of the heating furnace is pumped to the upper cooling tank and recirculated to bottom tank to maintain the inlet temperature at $300\,K$. The cooled water is then circulated to the heating chamber through a $0.25\,hp$ pump. A vacuum system containing a rotary pump and a diffusion pump connected in series is attached to the heating chamber, to maintain a vacuum level of 10^{-3} mm of Hg. The prepared specimens were heated up to the bonding temperature using induction furnace with a heating rate of 25°C/min; simultaneously the required pressure was applied. After the completion of bonding, the samples were cooled to room temperature and then removed from the chamber. By this procedure, Mg/Al joints were fabricated using different combinations of bonding temperature, bonding pressure and holding time. Lap shear tensile test was performed to evaluate shear strength of the joints and ram tensile test was conducted to evaluate bonding strength.

As the joints were not large enough for normal lap shear testing and ram tensile testing a non-standard test was devised to measure the shear strength and bonding strength of the bonds. Similar specimens were used by other investigator also (Ravisankar *et al.* 2009). The lap shear tensile specimens, as shown in Fig. 3 were prepared from the Mg/Al diffusion bonded joints by a electric spark line cutting machine (Make: ELECTROICA, Japan; Model: Super Cut-734) was used at a cutting speed of 1.5 mm/min and the prepared specimens are displayed in Fig. 4. Ram tensile specimens, as shown in Fig. 5, were prepared from the Mg/Al diffusion bonded joints by a spark
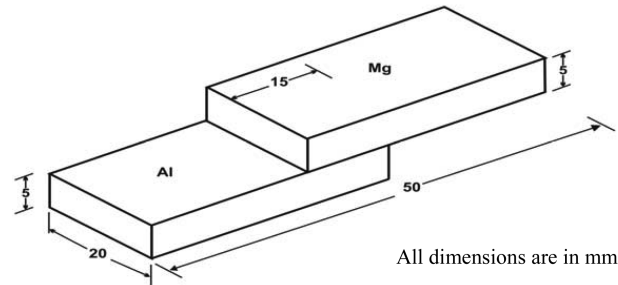
Fig. 3 Dimensions of lap shear tensile test specimen

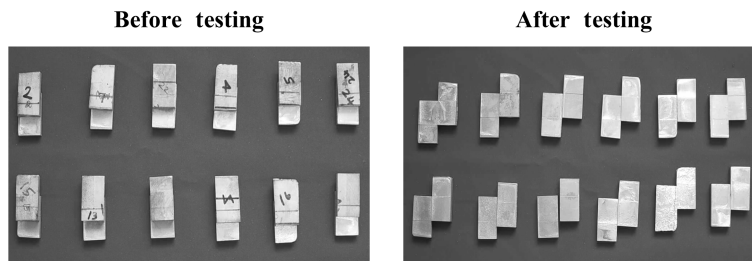**Before testing**　　　　　　　**After testing**

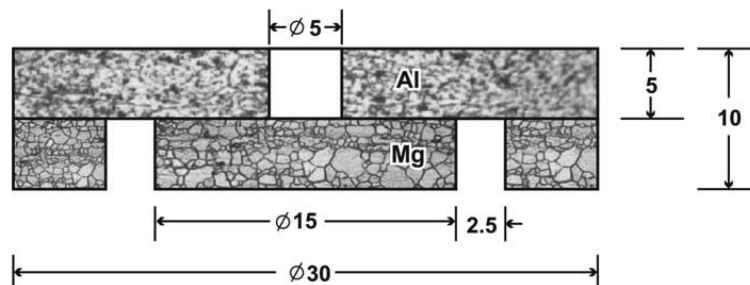Fig. 4 Photographs of lap shear tensile test specimen

Fig. 5 Schematic representation of ram tensile test specimen

erosion machine (Make: ELEKTRA, Japan; Model: Cut-500). The ram tensile test setup is shown in Fig. 6. Both lap shear and ram tensile test were carried out in 100 kN capacity servo controlled universal testing machine (Make: FIE-BLUESTAR, India; Model: UNITEK 94100) at a constant ram speed of 5 mm/min. Fig. 7 displays the ram tensile test specimens.

A transverse cross section of the specimen was extracted from each joint and was subjected to conventional metallographic preparations to reveal the various features of the joints. The microstructural analysis was carried out to measure the thickness of diffusion layer at the interface of the joints using light optical microscope (Make: MEIJI, Japan; Model: MIL-7100) and scanning electron microscope (Make: JOEL, Japan; Model: 5610 *LV*). The magnesium side was etched with a solution containing ethanol, picric acid, acetic acid and water whereas the aluminium side was etched with Keller's solution to reveal the microstructure. Vickers's microhardness testing machine (Make: SHIMADZU, Japan; Model: HMV-*T*1) was employed with 0.5 kg load for measuring the diffusion layer hardness as shown
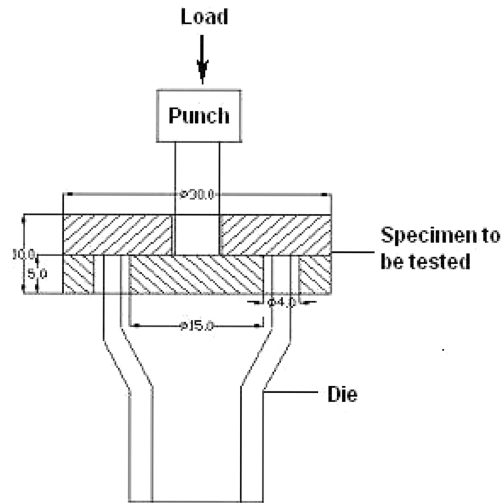
Fig. 6 Ram tensile test set up

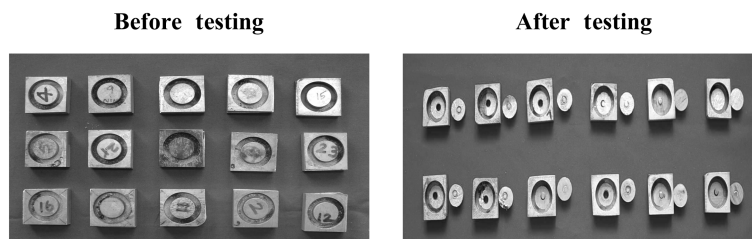**Before testing**   **After testing**

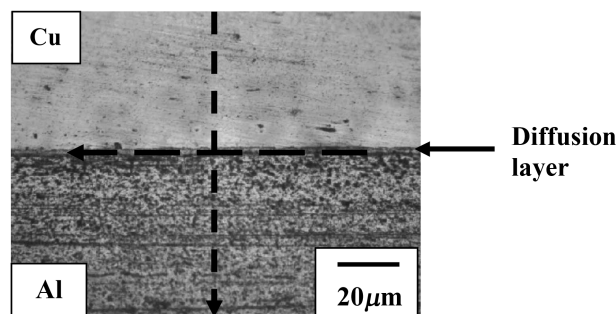
Fig. 7 Photographs of ram tensile test specimens

Fig. 8 Microhardness taken at different zones

in Fig. 8. Five readings were taken along the interface of the joint at close proximity distance and mean values are used for further analysis. Microhardness was also measured across the joint (normal to the interface region) in selected specimens to understand the hardness variation.

Energy dispersive spectrum (EDS) analysis was carried out using scanning electron microscope (Make: JEOL and Model: 5610 *LV*) at high magnification to estimate the weight percentage of elements, which are diffused at the interface zone and its adjacent sides of the bonded joints. To identify the phase constitution near the interface of the diffusion bonded joints, few selected

samples were cut from the transition region of both the sides and XRD analysis was carried out. The X-ray diffraction faces in the test are shown in Fig. 9. The XRD analysis was carried out in Theta-Theta (Vertical type), *D*/Max (Make: RIGAKU, Japan; Model: ULTIMA-III) with copper target under a working voltage of 40 kV and 40 mA working current. Scintillation counter detector was used with a scan range 3 to 154 deg (min. setup size 0.0002 deg). The results obtained are compared with data from the Joint Committee on Powder Diffraction Standards (JCPDS).
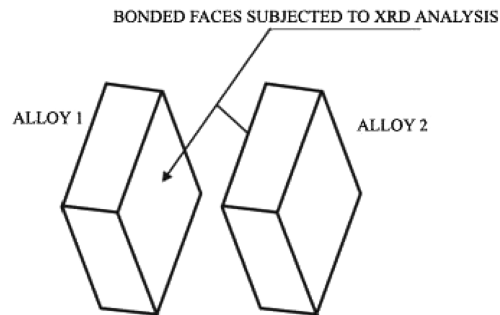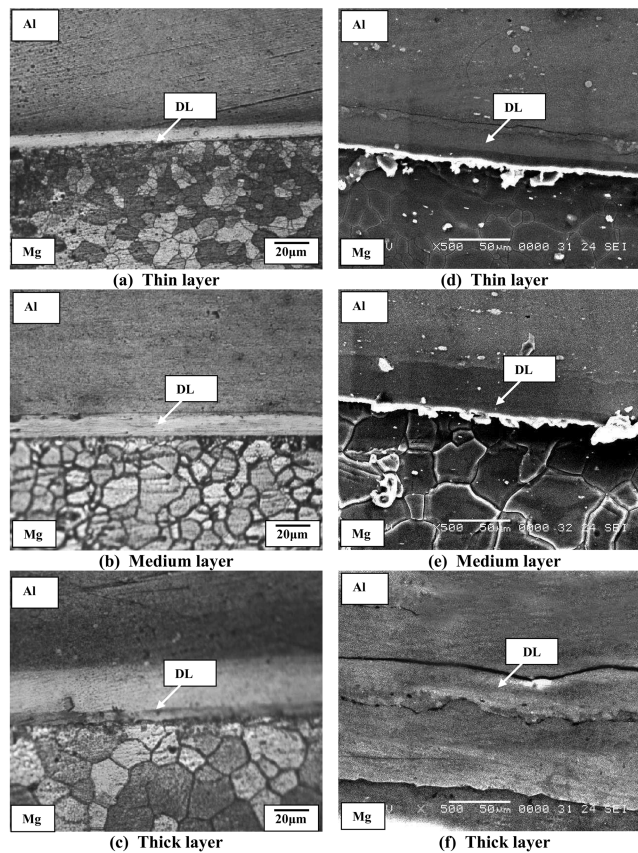

Fig. 9 X-ray test specimen details

Fig. 10 Optical and SEM micrographs of Mg/Al bonds (*a-c*: OM; *d-f*: SEM)

Table 3 Characterisation results of Mg/Al bonds

Bond type	T (ºC)	P (MPa)	t (min)	DL (μm)	IH (Hv)	SS (MPa)	BS (MPa)	EDS results Mg	EDS results Al	XRD results
Thin	420	8	30	27	112	25	45	51.52	39.28	$MgAl_2O_4$, Mg_2SiO_4 Al_2SiO_5
Medium	440	12	70	31	130	49	69	35.17	60.99	$MgSiO_3$, $MgAl_2O_4$, $MgSiO_4$, Mg_2Al_3, Mg_2Al_2
Thick	480	16	50	37	158	45	66	17.55	72.62	$MgAl_2O_4$, $Mg_2Al_2O_4$, Mg_2Al_3, $MgSiO_4$

Element	Weight%
Mg K	51.52
Al K	39.28
Total	100.00
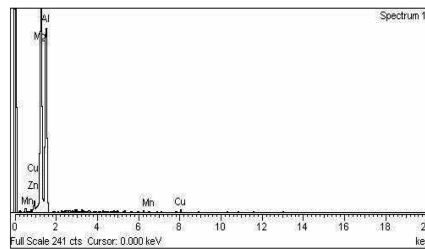
(a) Thin layer

Element	Weight%
Mg K	35.17
Al K	60.99
Cu K	2.72
Zn K	0.04
Total	100.00
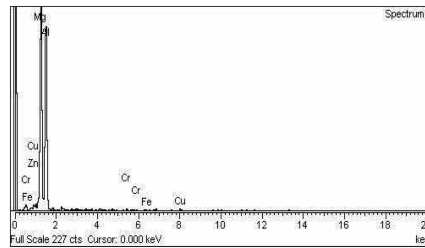
(b) Medium layer
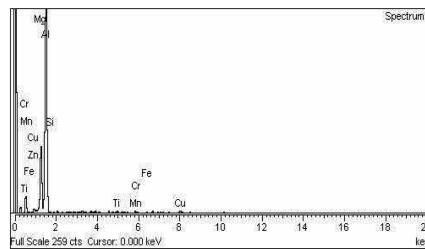
Element	Weight%
Mg K	17.55
Al K	72.62
Cu K	4.91
Zn K	0.11
Total	100.00

(c) Thick layer

Fig. 11 EDS results at the interface region of Mg/Al bonds

3. Results

Fig. 10 represents OM and SEM micrographs of interface of the joints fabricated using the process parameters presented in Table 3. Microhardness was measured at the joint interface at five different locations and the average value is presented in Table 3. Shear strength and bonding strength of the joints were evaluated and the values (average of 3 results) are presented in Table 3.
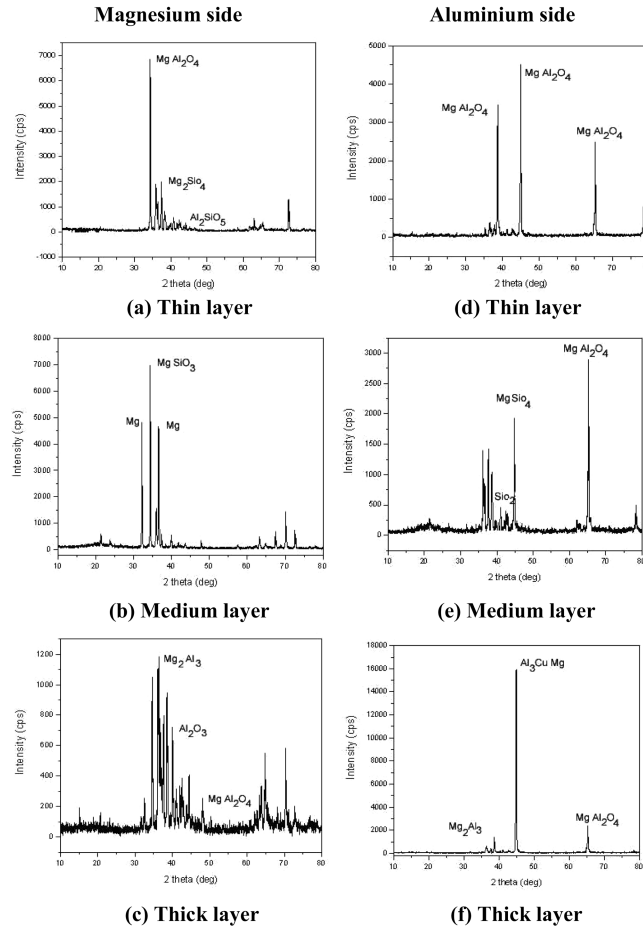
Fig. 12   X-ray diffraction (XRD) patterns for Mg/Al bonds

EDS analysis was carried out at the interface and the results are presented in Fig. 11. XRD analysis was carried out at the interface and results presented in Figs. 12 and 13. From the results presented in Table 3 and the Fig. 10 the following observations can be obtained:

(1) A very thin layer of thickness 27 μm was formed under the bonding temperature of 420ºC, holding time of 30 minute and bonding pressure of 8 MPa. This interface recorded a hardness of 112 *Hv* and exhibited shear strength and bonding strength of 25 MPa and 45 MPa respectively. The interface contains 51.52% of Mg and 39.28% of Al along with the intermetallic phases of $MgAl_2O_4$, Mg_2SiO_4 and Al_2SiO_5.

(2) A medium thick diffusion layer of 31 μm was formed under the bonding temperature of 440ºC, holding time of 70 minutes and bonding pressure of 12 MPa. This interface recorded a hardness of 130 *Hv* and exhibited shear and bonding strength of 49 MPa and 69 MPa, respectively. The interface contains 35.17% of Mg and 60.99% of Al along with the intermetallic phases of $MgSiO_3$, $MgAl_2O_4$, $MgSiO_4$, Mg_2Al_3 and Mg_2Al_2.

(3) A very thick diffusion layer of 37 μm was formed under the bonding temperature of 480ºC, holding time of 50 minutes and bonding pressure of 16 MPa. This interface recorded a hardness of
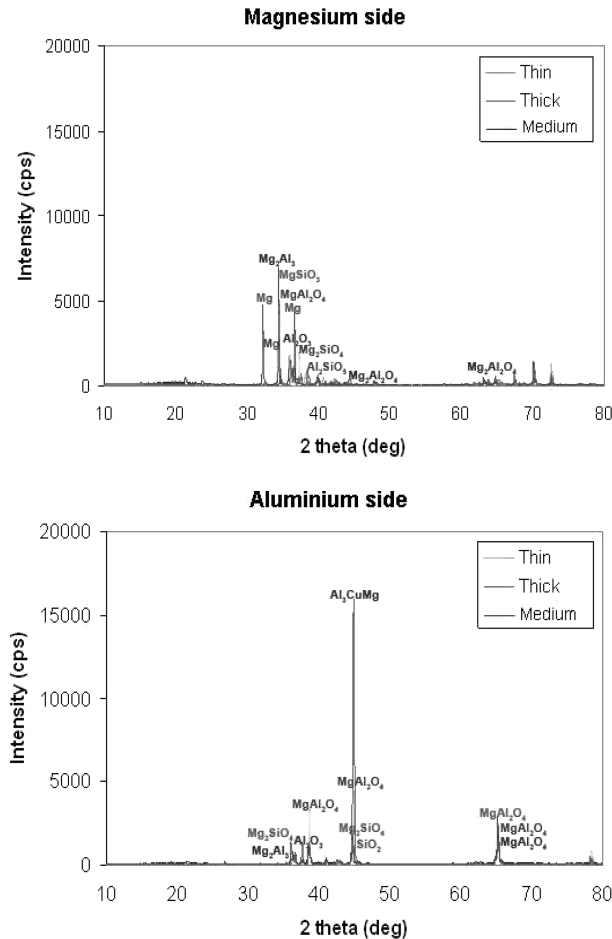
Fig. 13 XRD results for Mg/Al diffusion bonds

158 *Hv* and exhibited shear and bonding strength of 45 MPa and 66 MPa, respectively. The interface contains 17.55% of Mg and 72.62% of Al along with the intermetallic phases of $MgAl_2O_4$, $Mg_2Al_2O_4$, Mg_2Al_3 and $MgSiO_4$.

(4) Bonding temperature, bonding pressure and holding time have directly proportional relationship with diffusion layer thickness (*DL*) and interface hardness (*IH*). Interface hardness is showing directly proportional relationship with diffusion layer thickness.

(5) Diffusion of magnesium atoms showed an inversely proportional relationship with bonding temperature, bonding pressure and holding time. This is evident from weight percentage of magnesium elements at the interface (Table 3 - EDS results).

(6) Diffusion of aluminium atoms showed a directly proportional relationship with the bonding temperature, bonding pressure and holding time. This is evident from weight percentage of aluminium elements at the interface (Table 3 - EDS results).

(7) Maximum shear strength and bonding strength were exhibited by the joint which contained medium diffusion layer thickness (31 μm). Both the joints with thin (27 μm) and thick (37 μm) diffusion layers exhibited lower shear strength and bonding strength compared to the joints with
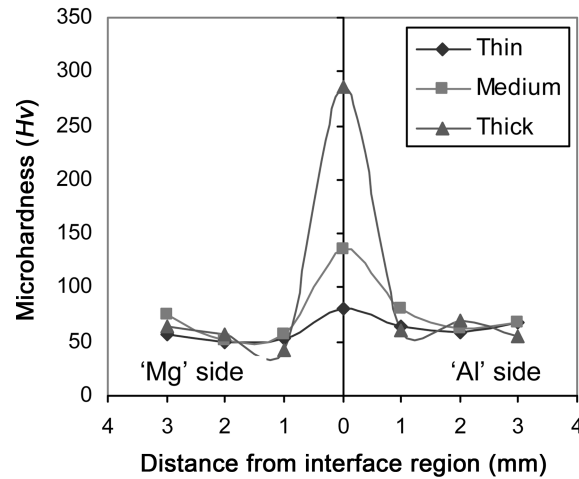
Fig. 14 Microhardness survey across the interface region

medium diffusion layer.

(8) Presence of Mg_2Al_3 and Mg_2Al_2 at the interface of the medium diffusion layer enhances the hardness and strength of these joints compared to the joints with thin and thick layers.

(9) Microhardness was also measured across the interface of Cu/Al, Mg/Al, Mg/Cu joints (perpendicular to the diffusion layer) at the different locations and the results are presented in Fig. 14. EDS analysis was also carried out at three different locations and the results are presented in Table 3. From the microhardness and EDS results, following inferences can be obtained.

(10) Hardness is maximum at the interface, irrespective of thickness of the diffusion layer. This may be due to the formation of intermetallic compounds at the interface.

(11) Thick diffusion layer recorded maximum hardness at all locations. This may be due to higher level of bonding temperature, bonding pressure and holding time used to fabricate the joints.

(12) Very near to the interface region (approximately 1 mm from the interface region on both the sides), an appreciable reduction in hardness was recorded in all the joints. This may be due to the depletion of respective atoms, which are diffused into the interface region to form intermetallic compounds. This was confirmed by EDS results presented in Table 3.

(13) The atomic radii of Al and Mg are 0.143 nm and 0.159 nm respectively. Since, the atomic radius of 'Al' is less than 'Mg', 'Al' migrates towards 'Mg' side in Mg/Al joints.

4. Discussion

The formation of diffusion layer depends on atomic diffusion. When the bonding temperature was increased to the required level, the joining processes have allowed the diffusion of all elements from both the sides quickly.

This fact promotes the chemical joint (in all welding condition) between materials, when inter-diffusion between the materials is provided without the formation of voids and brittle phases such as intermetallic compounds. These findings are in agreement with Fick's second law; a partial differential equation describes that the rates at which atoms are redistributed in a material by

diffusion (Li *et al.* 2012, Juan *et al.* 2008). The composition, extent, nature and properties of the phases originated during the welds, will control the resulting mechanical properties. The intermetallic compound grows steadily and gradually via enhanced temperature, at the bond region of dissimilar metal joints.

The particle distribution of intermetallic compounds has no harmful effects on the joint performances; moreover, it can strengthen the joints. The intermetallic compounds have never joined up and formed a whole body; they also have no effect on the plasticity and strength of joints. But once they connect and thickness grows beyond 5 μm, the plasticity and strength of joints will obviously be decreased. Because of diffusion rate for Al atoms is much higher than that of Mg atoms at high temperature, an excess of Al atoms diffuses across the interface into the magnesium side and forms cavities according to Kirkendall effect (Kundu *et al.* 2012). This Kirkendall effect leads to produce continuous cavities at the interface, resulting in a drastic reduction in the interface bonding strength level in the specimens bonded at maximum temperature.

The thickness of the intermetallic compound increases remarkably with holding time. Minimum holding time does not allow atoms to diffuse each other and hence diffusion layer thickness is very minimum. When holding time increased to maximum level grain boundary vibration will be more, this allows more atoms to diffuse on the other side leads to increase of diffusion layer thickness. Increase in hardness with increase in temperature and holding time can be attributed to the formation of intermetallic compounds as discussed above (Jian *et al.* 2012).

4.1 Effect of bonding temperature

Shear strength and bonding strength of the joints are increasing with increasing bonding temperature (Table 3). At a low bonding temperature, the shear strength and bond strength of the diffusion-bonded joint are low. This may be due to poor contact of the bonded surface and low thermal excitation. The bonding reaction is based on atoms diffusion and it is higher at higher bonding temperature. Bonding temperature improves the contact ratio and shear strength. Also, at low temperature, the flowability of metal is substantial yet yield strength of the base materials still remains high which, leads to an incomplete coalescence of the mating surfaces (Suleyman *et al.* 2012). Moreover, the grain boundary surface tension and grain boundary mobility are less at low temperature and these are the controlling factors for the initial movement of interface grain boundaries. At low temperature, boundary mobility is relatively low (Juan *et al.* 2008). Also with increase in temperature, the yield strength of the joint decreases, this result in larger interfacial deformation, and the atomic diffusivity increases, results in easier and speeder chemical bonding. Therefore, the joint strength increases with increase in bonding temperature.

When diffusion-bonding temperature increases, there is an increase in shear strength and bonding strength. Increase in diffusion bonding temperature promotes mass transfer of alloying elements across the interface, which is responsible for the increase in volume fraction of the reaction products; hence causes more embrittlement to the joints. However, plastic collapse of the mating surface asperities leads to intimate contact, which counter balances the embrittlement phenomena due to intermetallic phases; shear strength and bond strength naturally improves and attains maximum value (Widodo *et al.* 2012).

In contrast, at high temperature the initial stages of bonding could involve migration of interface grain boundaries as above, the higher rate of grain growth would lead to rapid removal of evidence of the bond line and increases the strength nearer to the parent metal.

Increase in the bonding temperature to maximum, the thickness of the intermetallic compound increases quickly. Quick increase in thickness of intermetallic compound leads to decrease in the strength and an increase in the brittleness of the joint. Further increase in temperature, the width of brittle intermetallics considerably increases and the embrittlement effect over-balances the positive effect obtained due to betterment in coalescence of faying surfaces (Masahashi *et al.* 2008). So, both the shear and bond strength drops to a minimum value.

4.2 Effect of bonding pressure

From the Table 3, it can be inferred that the shear strength and bonding strength of the joints are increasing with increase in bonding pressure, irrespective of bonding temperature and holding time. At low bonding pressure of 4 MPa, shear strength and bonding strength are minimum. Because, at low bonding pressure, contact is only at the protrusions on the bonded surface, so the contact rates and the strength of the bonded joint are lower. Generally, when the bonding pressure is applied, the points of contact between the two surfaces will expand almost instantaneously. When it is increased to 12 MPa, plastic deformation will develop at contact sites to increase the contact areas of clean surfaces and hence joint rate changes appreciably.

Further, increase of pressure to 20 MPa, results in small increase in shear strength and bonding strength. Increase in pressure influences re-crystallization temperature and deformation tends to enhance the contact of bond surface and rapid growth of re-crystallization. This will obviously increase the rate of interface contact and atoms are made to pass through this bonding interface. So, more diffusion paths are created due to movement of atoms. Even though, both copper and aluminium has f.c.c structures the diffusivity value of copper is greater than that of aluminium. This leads to increase in movement of more number of copper atoms towards the aluminium side. The movement of atoms will increase voids named as Kirkendall effect (Li *et al.* 2008). The voids produced during bonding would reduce the joint property.

The property of the bonded joints also mainly depends on thickness of the intermetallic compounds, which was unaffected as pressure increases (Tanaba *et al.* 2007). The voids formed at the original interface will disappear as the contact area expands with time, because the stress within the contact zone will cause a plastic flow by either conventional creep or super plasticity. The smaller voids would be removed rapidly by diffusion (Kenevisi *et al.* 2012).

4.3 Effect of holding time

The shear strength and bonding strength of the joints are increasing with increase in holding time, irrespective of temperature and pressure (Table 3). High shear strength is obtained at a holding time of 50 minutes for Cu/Al bonds. Holding time has an effect on the creep of the protrusions and the quantity of atomic diffusion (Hunta *et al.* 2012). Shear strength and bonding strength of the joint increases with increasing holding time. If holding time is not sufficient to allow diffusion of atoms across the bond interface from the mating surfaces, the strength will be lower. The strength increased more rapidly with increasing holding time up to 50 minutes and then it decreases sharply. Longer holding times showed a continuing grain growth accompanied by a small increase in specific strength. The sharp decrease in strength was attributed to the growth of intermetallic compounds (Kenevisi and Mousavi khoie 2012, Aydýn *et al.* 2012). The thickness of the intermetallic compound increases remarkably with holding time and the tensile strength of the bond joint decreases.

5. Conclusions

From this investigation, the following important conclusions are derived.

1. Diffusion bonding process parameters such as bonding temperature, bonding pressure and holding time are having directly proportional relationship with diffusion layer thickness and interface hardness. However, the effect of bonding pressure on bond characteristics is very minimal compared to bonding temperature and holding time.

2. The thickness of diffusion layer plays an important role in deciding bonding strength and shear strength of the dissimilar joints. Insufficient diffusion bonding process parameters led to the formation of very thin diffusion layer at the interface, subsequently led to weak bonding (low strength).

3. Excessive diffusion bonding process parameters led to the formation of very thick diffusion layer, which in turn led to brittle interface, subsequently yielded weak bonding (low strength). Usage of optimized diffusion bonding process parameters led to the formation of medium thick diffusion layer, which exhibited higher bonding strength and shear strength.

References

Bakhtiaria, R., Ekramia, A. and Khanb, T.I. (2012), "The effect of TLP bonding temperature on microstructural and mechanical property of joints made using FSX-414 super alloy", *Mater. Sci. Eng. A,* **546**(1), 291-300.

Huga, A., Dornc, C.K. and Abdoua, M. (2012), "Diffusion bonding beryllium to reduced activation ferritic martensitic steel: Development of processes and techniques", *Fusion Eng. Des*., dx.doi.org/10.1016/ 2012.04.010

K., Aydın, Y., Kaya and N., Kahraman (2012), "Experimental study of diffusion welding/bonding of titanium to copper", *Mater. Design*, **37**, 356-368.

Kenevisi, M.S. and Mousavi Khoie, S.M. (2012), "An investigation on microstructure and mechanical properties of Al 7075 to Ti–6Al–4V Transient Liquid Phase (TLP) bonded joint", *Mater. Des*, **38**, 19-25.

Kenevisi, M.S. and Mousavi Khoie, S.M. (2012), "A study on the effect of bonding time on the properties of Al7075 to Ti–6Al–4V diffusion bonded joint", *Mater. Lett*, **76**(1), 144-146.

Kundu, S., Roy, D., Chatterjee, S., Olson, D. and Mishra, B. (2012), "Influence of interface microstructure on the mechanical properties of titanium/17-4 PH stainless steel solid state diffusion bonded joints", *Mater. Design*, **37**, 560-568.

Li, W.H. and Joelle Ong, S.W. (2012), "Cu diffusion in Ag-plated Cu leadframe packages", *Microelectron. Reliab*., **52**(7), 1523-1527.

Li, Z.F., Dong, J., Zeng, X.Q., Lu, C., Ding, W.J. and Ren, Z.M. (2007), "Influence of strong magnetic field on intermediate phase growth in Mg-Al diffusion couple", *J. Alloy. Compd*., **440**(1-2), 132-136.

Masahashi, N., Semboshi, S., Konno, T.J. and Hanada, S. (2006), "Effect of pressure application on micro structure evolution in a composite of Fe–Al alloy and Cr Mo steel", *J. Alloy. Compd*., **413**(1-2), 281-288.

P., Zhang, J., Zhao and B., Wenb (2012), "Retention and diffusion of H, He, O, C impurities in Be", *J. Nucl. Mater*., **423**(1-3), 164-169.

P., Liu, Y., Li, H., Geng and J., Wang (2006), "Investigation of interfacial structure of Mg/Al vacuum diffusion bonded joint", *Vacuum*, **80**(5), 395-399.

Ravisankar, B., Krishnamoorthi, J., Ramakrishnan, S.S. and Angelo, P.C. (2009), "Diffusion bonding of SU 263", *J. Mater. Process. Tech*, **209**(4), 2135-2144.

S., Ozcan, A., Ozcifci, S., Hiziroglu and H., Toker, (2012), "Effects of heat treatment and surface roughness on bonding strength", *Constr. Build. Mater.,* **33**, 7-13.

Tanaba, U.J., Sasaki, T. and Kishi, S. (2007), "Diffusion bonding of Ti/graphite and Ti/ diamond by hot isostatic pressing method", **192-193**, 453-458.

W.W., Basuki, O., Kraft and J., Aktaa (2012), "Optimization of solid-state diffusion bonding of Hastelloy C-22 for micro heat exchanger applications by coupling of experiments and simulations", *Mater. Sci. Eng. A*, **538**, 340-348.

W., Deqing, S., Ziyuan and Q., Ruobin (2007) "Cladding of stainless steel on aluminium and carbon steel by inter layer diffusion bonding", *Scripta Mater,* **56**(5), 369-372.

W., Juan, L., Yajiang, L., Penga and G., Haoranb (2008), "Microstructure and XRD analysis in the interface zone of Mg/Al diffusion bonding", *J. Mater. Process. Tech.*, **205**(1-3), 146-150.

Y., Li, P., Liu, J., Wang and H., Ma, (2008), "XRD and SEM analysis near the diffusion bonding interface of Mg/Al dissimilar Materials", *Vacuum,* **82**(1), 15-19.

Z., Jian, S., Qiang, L., Guoqiang, L., Meijuan and Z., Lianmeng, (2012), "Microstructure and bonding strength of diffusion welding of Mo/Cu joints with Ni interlayer", *Mater. Design*, **39**, 81-86.